ACS APPLIED MATERIALS & INTERFACES

Research Article

www.acsami.org

Atomic Layer Deposition of Al-Doped ZnO/Al_2O_3 Double Layers on Vertically Aligned Carbon Nanofiber Arrays

Gary A. Malek,*[,†] Emery Brown,[‡] Steven A. Klankowski,[‡] Jianwei Liu,[†] Alan J. Elliot,[†] Rongtao Lu,[†] Jun Li,[‡] and Judy Wu*[,†]

[†]Department of Physics and Astronomy, University of Kansas, Lawrence, Kansas 66045, United States

[‡]Department of Chemistry, Kansas State University, Manhattan, Kansas 66506, United States

Supporting Information

ABSTRACT: High-aspect-ratio, vertically aligned carbon nanofibers (VACNFs) were conformally coated with aluminum oxide (Al_2O_3) and aluminum-doped zinc oxide (AZO) using atomic layer deposition (ALD) in order to produce a three-dimensional array of metal−insulator−metal core−shell nanostructures. Prefunctionalization before ALD, as required for initiating covalent bonding on a carbon nanotube surface, was eliminated on VACNFs due to the graphitic edges along the surface of each CNF. The graphitic edges provided ideal nucleation sites under sequential exposures of H_2O and trimethylaluminum to form an Al_2O_3 coating up to 20 nm in thickness. High-resolution transmission electron microscopy (HRTEM) and scanning electron microscopy images confirmed the conformal core−shell AZO/Al_2O_3/CNF structures while energy-dispersive X-ray spectroscopy verified the elemental composition of the different layers. HRTEM selected area electron diffraction revealed that the as-made Al_2O_3 by ALD at 200 °C was amorphous, and then, after annealing in air at 450 °C for 30 min, was converted to polycrystalline form. Nevertheless, comparable dielectric constants of 9.3 were obtained in both cases by cyclic voltammetry at a scan rate of 1000 V/s. The conformal core−shell AZO/Al_2O_3/VACNF array structure demonstrated in this work provides a promising three-dimensional architecture toward applications of solid-state capacitors with large surface area having a thin, leak-free dielectric.

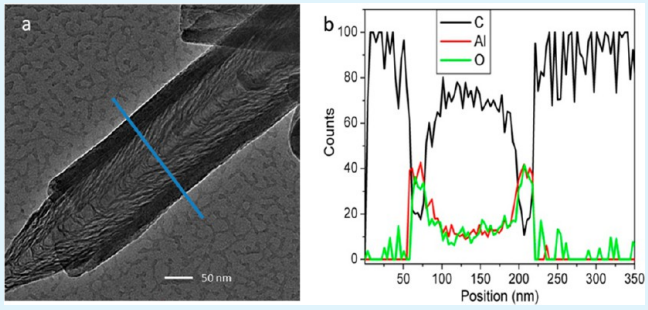

KEYWORDS: *vertically aligned carbon nanofiber array, atomic layer deposition, core−shell nanostructure, 3D electrode, conformal coating*

1. INTRODUCTION

Three-dimensional (3D), carbon-based nanostructures have unique advantages for energy applications because of their desirable electrical properties, large surface-to-volume ratio, low specific mass, and relatively large abundance.[1−3] Among the 3D, carbon-based nanostructures, vertically aligned carbon nanofibers (VACNFs) grown as arrays on conductive substrates provide an ideal 3D electrode that is most desirable for many energy device applications including dye-sensitized solar cells,[4] hybrid supercapacitors,[5] and lithium-ion batteries.[6] The VACNFs can be easily grown to tens of micrometers in length, vary from 50 to 150 nm in diameter (~100:1 aspect ratio), and have an areal density of 1×10^9 CNFs/cm^2 providing a significantly enhanced electrode surface area.

Conformal coating of functional materials on VACNF arrays is required for applications that take advantage of the large surface area. However, for high-aspect-ratio vertical structures, conformal coating can be quite challenging due to shadow effects from most deposition techniques. Atomic layer deposition (ALD) provides an ideal method for solving this problem. In particular, ALD allows atomic-scale thickness control of the conformal coating because of its self-terminating, layer-by-layer growth mechanism.[7] Progress has been made recently in coating 3D structures using ALD. For example, Banerjee et al. reported successful ALD coating of anodized aluminum oxide (Al_2O_3) nanotubes with a 200:1 aspect ratio in order to fabricate TiN/Al_2O_3/TiN metal−insulator−metal capacitors.[8] In addition, Kemell et al. utilized ALD to conformally coat Si micropores with a 25:1 aspect ratio in order to fabricate Si/Al_2O_3/Al-doped ZnO (AZO) capacitor arrays.[9] The atomic-scale thickness control provided by ALD in these examples was advantageous in achieving extremely thin dielectric layers on the order of several nanometers as illustrated by the high capacitances reported.

ALD is a chemical process and requires well-defined surface functional groups for atomic layer nucleation during alternating exposures of chemical precursors. When these functional groups are not readily available, such as the case with carbon

Received: January 30, 2014
Accepted: April 1, 2014
Published: April 1, 2014

   dx.doi.org/10.1021/am5006805 | ACS Appl. Mater. Interfaces 2014, 6, 6865−6871

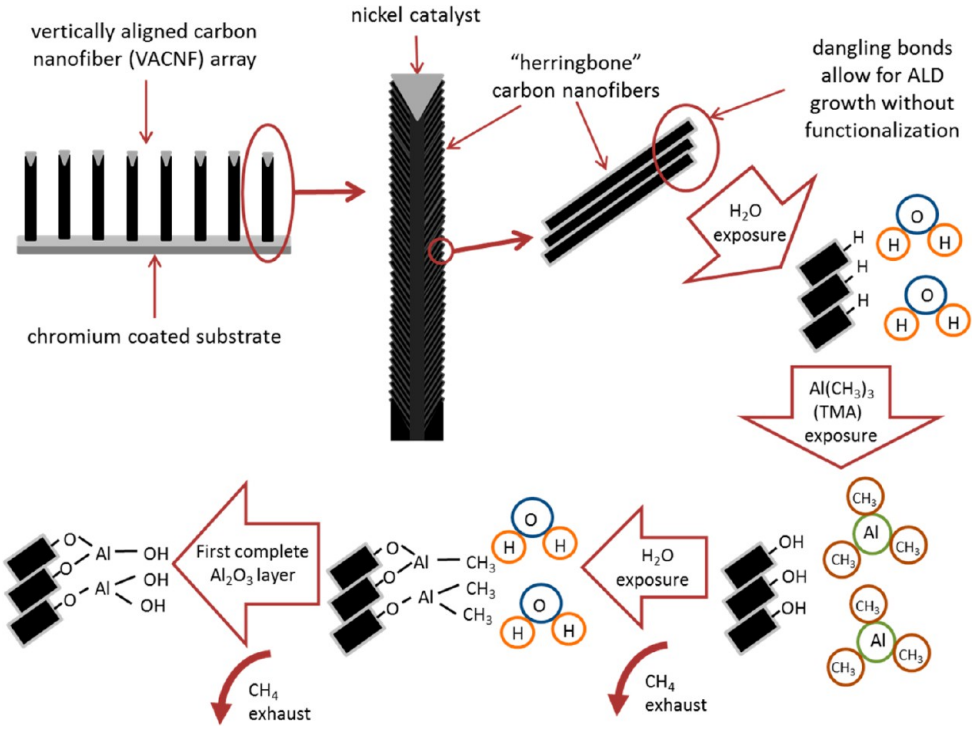

Figure 1. Schematic of one complete Al_2O_3 ALD cycle along the sidewall of a CNF.

nanotubes (CNTs) that have chemically inert sidewalls,[10] ALD coating cannot be carried out unless the CNT sidewalls are covalently or noncovalently functionalized beforehand. Covalent functionalization requires the formation of defect sites where nucleation occurs, but with this process, the electrical transport properties of the CNTs are seriously degraded due to charge carrier scattering by the generated defects. Additionally, ALD growth after covalent functionalization will not be completely uniform since the defect site locations are randomly distributed throughout the CNTs.[11] Noncovalent functionalization does not create defect sites, but it does require additional procedural steps and chemicals leading to higher cost and longer fabrication time.[12] Unlike CNTs, VACNFs consist of conically stacked graphitic cups with dangling carbon bonds on the outer rims which are distributed along the sidewalls of the fiber.[13,14] These dangling bonds along the graphitic edges are quickly converted into C−H and C−OH bonds once exposed to air and can serve as ideal nucleation sites for coating of functional materials by ALD which eliminates the need for covalent or noncovalent functionalization.[15−17] In addition, VACNFs have highly conductive metallic properties (with a resistivity of $(6.3 \pm 1.7) \times 10^{-4}$ Ω cm) in contrast to the mixed metallic and semiconductor properties of CNTs, and thus serve well as a current collector.[18]

In this work, we explore ALD fabrication of 3D, metal−insulator−metal core−shell nanostructures using pristine VACNF arrays as one of the metallic electrodes. The obtained conformal core−shell AZO/Al_2O_3/CNF structures represent the first successful double-layer ALD coatings on vertically aligned, 3D CNF arrays and are promising candidates for high-performance, solid-state capacitors.

2. EXPERIMENTAL DETAILS

VACNF arrays were grown on 1 cm × 2 cm silicon substrates coated with a 100 nm thick chromium barrier layer and a 22.5 nm thick nickel catalyst film. VACNF growth was accomplished using a DC-biased plasma enhanced chemical vapor deposition (PECVD) system (Black Magic PECVD System, AIXTRON) at 800 °C with a flowing mixture of C_2H_2 (at 63 sccm) and NH_3 (at 250 sccm) gas precursors at a processing pressure of ∼4.1 Torr following a previously published procedure.[4−6] The VACNF array samples used in this study have an average areal density of $\sim 1 \times 10^9$ CNFs/cm^2, with a diameter in the range of 50−150 nm and a length of 3−5 μm controlled by 20−30 min of growth time.

Figure 1 shows a schematic for the complete Al_2O_3 ALD growth cycle, including reaction byproducts, on a CNF sample. The Al_2O_3 ALD growth procedure and ALD reactor design are discussed extensively in previously published materials.[19−22] ALD Al_2O_3 films were grown using high-purity H_2O (optima grade, Fisher Scientific) and trimethylaluminum (TMA, $Al(CH)_3$; semiconductor grade, Akzo Nobel) as precursors. Ultrahigh purity (99.9999%) N_2 was used as the carrier and purging gas with a maintained flow rate of 5 sccm throughout all ALD cycles. The VACNF array substrates were heated to 200 °C for Al_2O_3 growth. ALD cycling began with a one-second H_2O exposure to further prepare the graphitic edges with hydroxyl groups for reaction with TMA. After the initial H_2O exposure, the ALD chamber and gas feeding lines were purged with N_2 for 30 s to prevent chemical vapor deposition occurrence during the TMA exposure. Following the N_2 purge, a one-second TMA exposure provided the aluminum atoms that bonded to the hydroxyl group oxygen atoms on the VACNF sidewalls. Another 30-s N_2 purge was then performed to clear the chamber and gas lines of any residual TMA. This process was repeated for a total of 200 cycles with a final exposure of H_2O to end with hydroxyl groups along the sidewalls. The as-grown Al_2O_3 is typically amorphous,[23] therefore, in order to improve the crystallinity of the Al_2O_3 layer, a coated VACNF array was thermally annealed in a tube furnace at 450 °C for 30 min and then cooled to room temperature.

To verify the integrity of the ALD Al_2O_3 film, we fabricated a planar capacitor. The base electrode composed of an n-doped silicon substrate coated with a 100 nm chromium layer on top. A 20 nm Al_2O_3 dielectric layer was grown on the chromium surface utilizing the ALD method mentioned previously. A top electrode was provided by sputtering 600 nm of palladium on a portion of the Al_2O_3 surface. Another planar sample, fabricated under the same conditions, was

annealed in a tube furnace using the same conditions as the VACNF array sample except at a temperature of 400 °C. The lower temperature was utilized in order to eliminate cracking of the film that appeared at the higher temperature. The top electrode for the thermally annealed sample was applied after annealing was performed.

ALD AZO was grown with the same precursors as before but with the addition of diethylzinc (DEZ, $(C_2H_2)_5Zn$; research grade, SAFC Hitech) while utilizing the 19:1 Zn/Al ratio as published by Kong et al.[24] in order to achieve the desired electrical conductivity. The Al_2O_3/VACNF array substrate was heated to 200 °C for AZO growth. The 200 ALD cycles consisted of 10 supercycles where each supercycle contained 19 cycles of alternating H_2O and DEZ for every one doping cycle of H_2O and TMA. Each precursor exposure was one second with a 30-s N_2 purge in between. The resistivity of the AZO film was determined by growth on a glass slide that was placed alongside the Al_2O_3/VACNF array during fabrication.

The structure and morphologies of the samples were examined using field-emission scanning electron microscopy (FESEM, FEI Nova SEM 430) at an electron beam accelerating voltage of 3.5 keV. High-resolution transmission electron microscopy (HRTEM) images and selected area electron diffraction (SAED) patterns were obtained using an FEI Tecnai F20 XT field-emission transmission electron microscope at 200 kV. The chemical composition and distribution of the core−shell structures were analyzed using energy dispersive X-ray spectroscopy (EDX). Electrical characterization was conducted on the planar capacitor using a 760D Bipotentiostat (CH Instruments Inc., TX). The specific capacitance was measured by cycling the bias voltage between −0.1 to +0.1 V at various scan rates, and the galvanostatic charge−discharge at selected current densities. The Ohmic resistance across the 20 nm thick Al_2O_3 dielectric layer was measured using AC impedance spectroscopy for further insight.

3. RESULTS AND DISCUSSION

The growth rate for Al_2O_3 on silicon oxide (SiO_2) for our system was previously determined to be approximately 0.11 nm/cycle by spectroscopic ellipsometry[21,22] and follows closely to other published results.[19,20] HRTEM images revealed that the inner shell of the ALD double-layer coated on a VACNF was ∼20 nm thick which is in agreement with the thickness anticipated from 200 ALD cycles of Al_2O_3 growth. This verified the assumption that nucleation of Al_2O_3 would occur directly along the graphitic edges of the VACNFs without need for functionalization. This confirmation is important since covalent functionalization of CNTs degrades charge mobility as well as conductivity of the CNTs, and noncovalent functionalization requires additional time and cost. Direct atomic layer bonding to VACNF surfaces using ALD growth has advantages in maintaining the high conductivity of the electrode, simplifying the device fabrication procedure, and generating cleaner interfaces between electrode surface and ALD materials with minimized surface defects and chemical contaminants. These advantages are critical toward fabrication of high-performance, 3D nanostructured devices utilizing VACNF arrays as part of the 3D electrode.

Additional HRTEM images also revealed that the outer 19:1 AZO layer of the ALD double-layer coating on the VACNFs was ∼33 nm thick. The corresponding growth rate of 0.17 nm/cycle is comparable to, but slightly less than, that reported by J. W. Elam et al. using similar conditions.[25,26] The resistivity of the 19:1 AZO on glass was approximately 4.2×10^{-3} Ω cm, which is within the expected values according to previously published results.[24,25,27] This resistivity corresponds to a sheet resistance of 1.3×10^3 Ω/□. In addition, this result suggests that aluminum doping of ZnO during the ALD supercycles was sufficient. Because AZO is a transparent conducting oxide, ALD of AZO will allow in situ fabrication of metal−insulator−metal multilayers on various substrates, especially to conformally coat VACNFs.

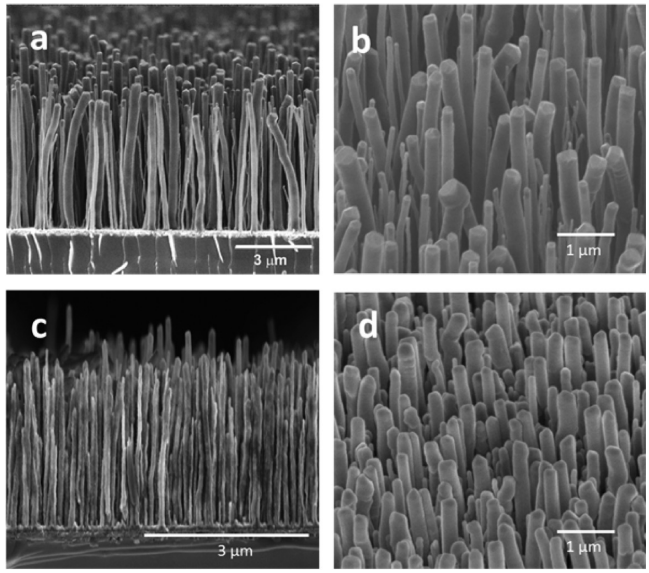

Figure 2. FESEM images of VACNF arrays. (a) Side view of an as-grown VACNF array on Si after cleavage. (b) 45° perspective view from top of an as-grown VACNF array with the Ni catalyst tip clearly visible. (c) Side view and (d) 45° perspective view from top of an AZO/Al_2O_3 coated VACNF array.

As depicted in images a (side view) and b (45° perspective view) in Figure 2, the FESEM images of as-grown CNFs reveal their vertically aligned nature with an approximate density of 1×10^9 CNFs/cm^2. The images also verify that the VACNF diameters are in the range of 50−150 nm with heights ranging from 3 to 5 μm. The nickel catalyst for each VACNF is clearly noticeable in Figure 2b as a bright spot on the fiber tip. After growth of the ALD AZO/Al_2O_3 double layer coatings, the nickel nanoparticles become less visible. The vertically aligned nature of each CNF is still apparent in both side view (Figure 2c) and 45° perspective view (Figure 2d). Additionally, Figure 2d clearly reveals an increase in VACNF thickness due to the ALD coatings. In particular, the AZO/Al_2O_3 double-layer coating appears highly uniform and conformal as expected for ALD.

To further confirm the conformal nature of the ALD core−shell structure, we took HRTEM images of individual Al_2O_3/VACNF samples. Images a and b in Figure 3 show the 20 nm Al_2O_3 conformal coating extending down the entire length of a VACNF to the point where it broke off of the metal base. As mentioned previously, this thickness is in agreement with spectroscopic ellipsometry data taken of ALD Al_2O_3 growth on SiO_2-coated silicon substrates. More importantly, the resulting Al_2O_3 thickness verifies the assumption that prefunctionalization of the VACNF surface is not required for ALD growth to occur. The graphitic edges on the VACNF sidewalls were sufficient nucleation sites for initiating ALD growth. Examining the scale bars of images a and b in Figure 3 reveals that the outer diameter of the Al_2O_3/VACNF core−shell structure is increased accordingly to a value of approximately 110 nm. The stacked conelike nature of a "herringbone" VACNF is apparent in each of the TEM images of Figure 3, and a closer examination of Figure 3b reveals the cone shape of the VACNF where it was pulled from the base. In addition to the type of VACNF core present, the 20 nm conformal shell coating

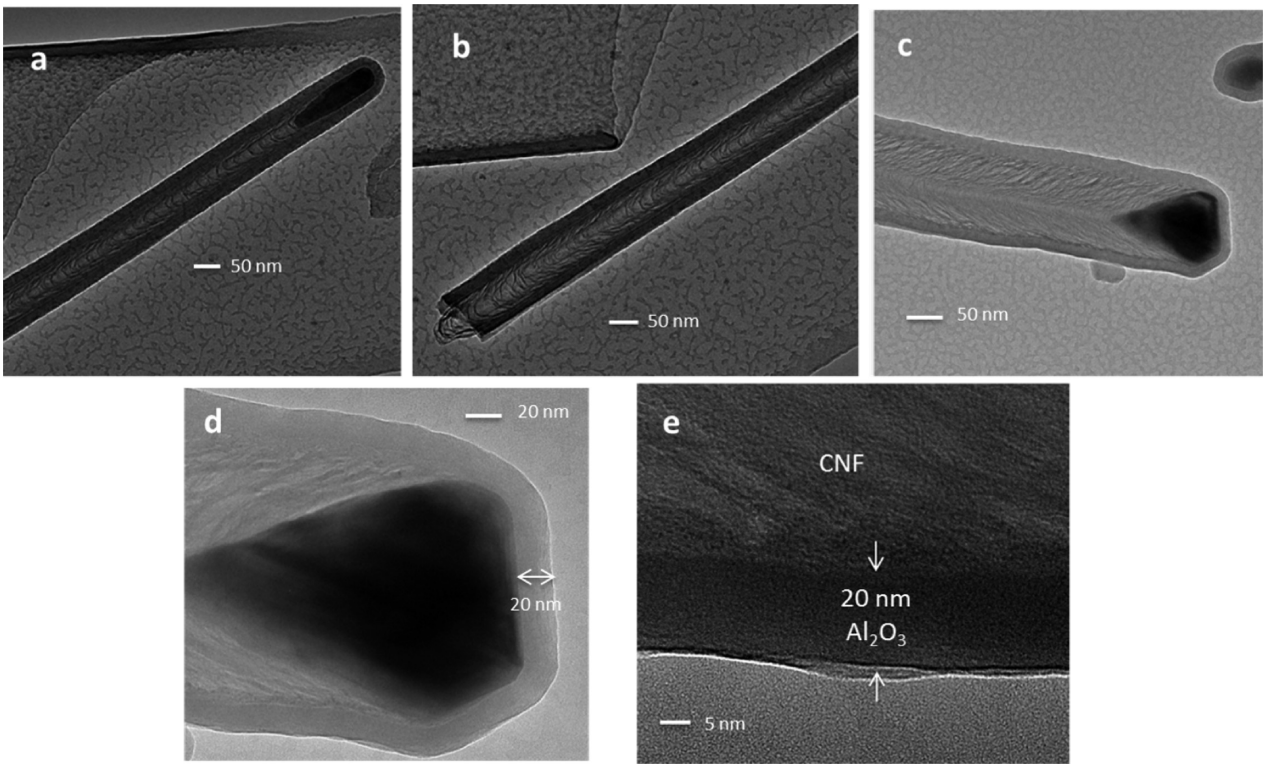

Figure 3. TEM images of (a) conformal Al_2O_3 coating along a CNF including the Ni catalyst tip. (b) Conformal Al_2O_3 coating continues down the shaft of the CNF up until the point where it was broken off from the base. (c) Conformal Al_2O_3 coating along another CNF which also shows the "herringbone" nature of the CNF. (d) Close-up of the conformal coating around the Ni tip. (e) Extreme close-up image of CNF core and Al_2O_3 shell.

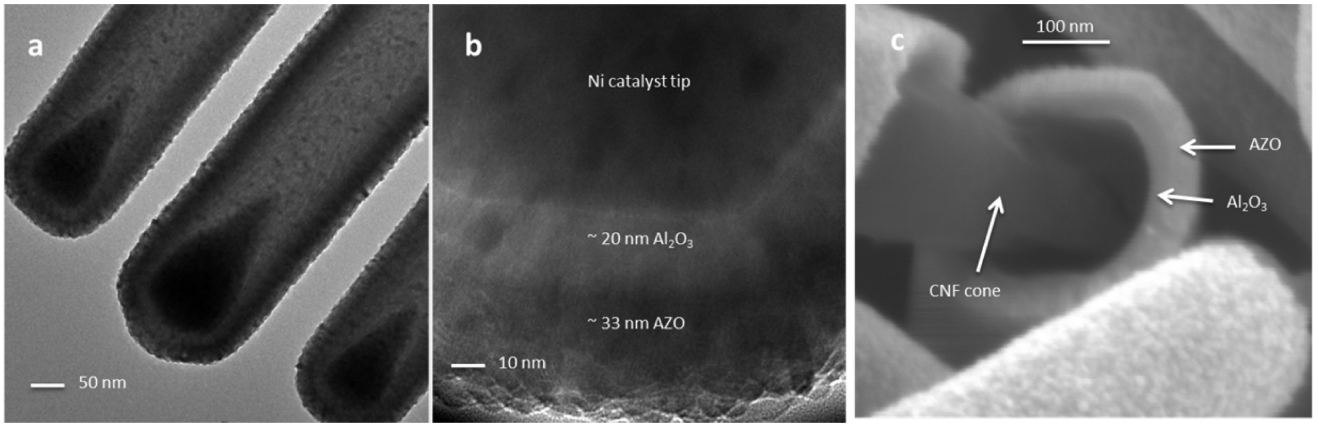

Figure 4. HRTEM images of multilayer ALD growth on VACNFs. (a) Multilayer Al_2O_3/AZO conformal coatings transition without problem from CNF to Ni catalyst tip. (b) HRTEM close-up of Ni/Al_2O_3/AZO layering. (c) FESEM image showing core−shell multilayer structure.

around the nickel catalyst tip is clearly shown in Figures 3a, c, and d. A close-up image of the VACNF transitioning to the amorphous Al_2O_3 shell is shown in Figure 3e, which again verifies the 20 nm thickness.

The HRTEM images of AZO/Al_2O_3 double-layer coated VACNFs are depicted in Figures 4a and 4b. These images reveal the expected growth of 20 nm Al_2O_3 on which a 33 nm AZO layer can be seen in a conformal shell along a portion of the VACNF with a complete capping of the nickel catalyst tip. A cross-section FESEM image of an AZO/Al_2O_3/VACNF sample (Figure 4c) verified the core−shell structure of the AZO/Al_2O_3 coating at the point that a coated VACNF was broken off by mechanical force. In addition to the conformal coating surrounding the VACNF, the conelike nature of the VACNF core is also apparent.

To further confirm that Al_2O_3 was indeed the material grown by ALD to form the inner shell, we obtained EDX data along a portion of a coated VACNF (Figure 5a). The elemental counts vs position graph indicate that the VACNF core has a diameter of ∼125 nm, whereas the whole core−shell structure after ALD coating has an outer diameter of ∼165 nm. The elemental analysis further revealed significant counts of aluminum and oxygen along the 20 nm thick sidewalls (Figure 5b). Furthermore, the carbon count is significantly larger inside the Al_2O_3 shell, which is expected because of the presence of the CNF.

dx.doi.org/10.1021/am5006805 | ACS Appl. Mater. Interfaces 2014, 6, 6865−6871

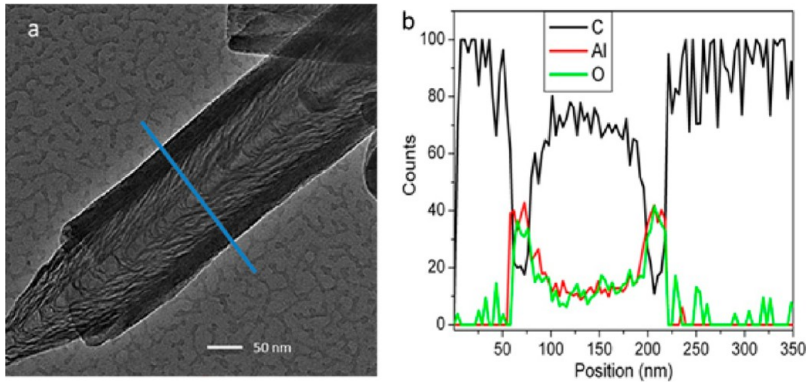

Figure 5. EDX elemental analysis. (a) HRTEM image of Al_2O_3/CNF with blue line showing scan region. (b) Elemental count vs position graph.

It has been shown that annealing an amorphous film can induce crystallization and convert an amorphous structure into a polycrystalline form.[28] To confirm this process, we obtained electron diffraction patterns from the selected area under HRTEM for preannealed (Figures 6a, b) and postannealed

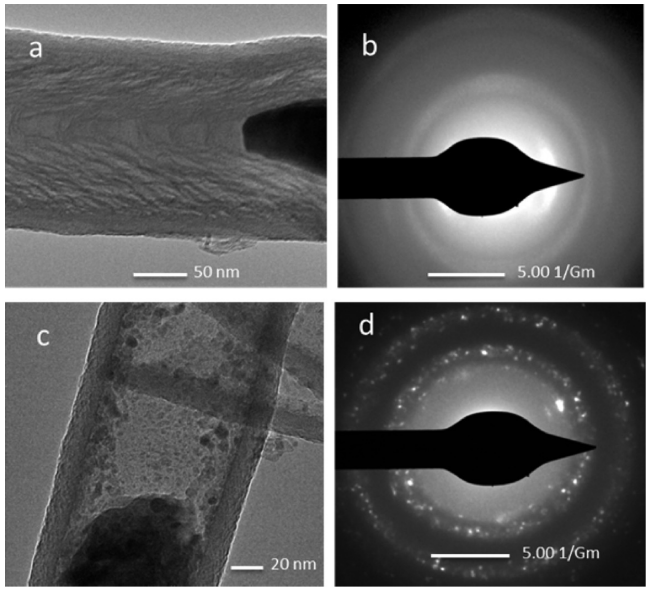

Figure 6. (a) Al_2O_3 coated CNF before annealing. (b) No diffraction pattern is present before annealing. (c) Al_2O_3 coated CNF after annealing. (d) Apparent diffraction pattern is present after annealing.

(Figures 6c, d) samples of Al_2O_3 coated CNFs. Only a ringlike diffusive diffraction pattern was produced for the preannealed sample (Figure 6b), confirming the as-made ALD Al_2O_3 to be amorphous. After annealing the same sample in air, a diffraction pattern with sharp spots on the diffusive rings formed (Figure 6d), verifying that the Al_2O_3 layer was now polycrystalline. This transformation may change the properties of the Al_2O_3 layer, which could be beneficial for some applications.

To assess the dielectric properties of ALD deposited Al_2O_3, we constructed two electrostatic planar capacitors with one using an unannealed Al_2O_3 layer and another with an annealed Al_2O_3 layer. Both capacitors had 2 mm × 2 mm lateral size with 20 nm Al_2O_3 dielectric layer deposited by ALD that was sandwiched between a 600 nm palladium top electrode and a 100 nm chromium bottom electrode on an n-doped silicon substrate. Electrostatic measurements were conducted to determine their specific capacitance and dielectric constants. Comparable dielectric constants as well as nearly identical capacitive behaviors were observed for both capacitors. Therefore, discussion is limited to only the annealed capacitor.

An ideal electrostatic capacitor has perfect rectangular shaped $I-V$ curves when the bias voltage is cycled between two voltage settings. Figure 7a shows the cycling $I-V$ curves of an annealed planar capacitor. The rectangular shapes indicate the near perfect capacitive behavior. Both the charging and discharging

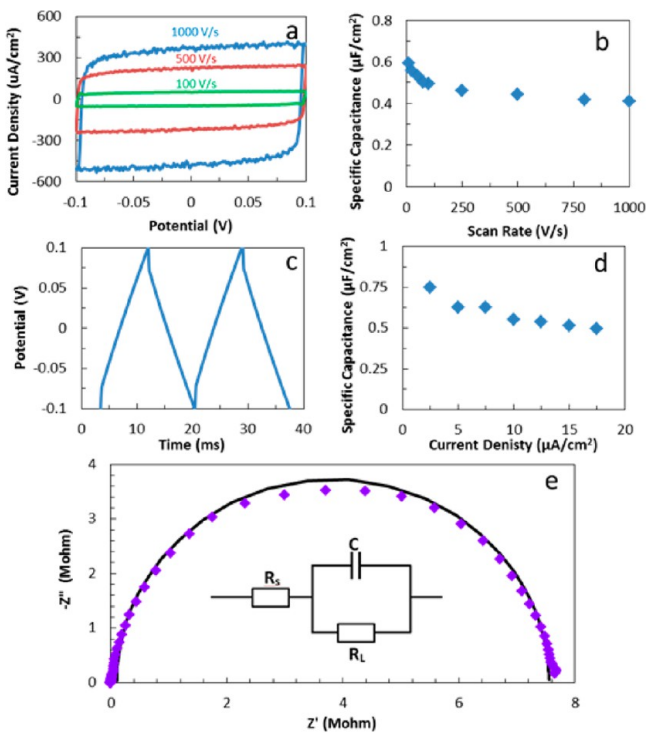

Figure 7. Electrical characterization of a planar capacitor. (a) $I-V$ curves measured by cycling the bias voltage between −0.1 to +0.1 V at the rates of 100, 500, and 1000 V/s, respectively. (b) The area-specific capacitance vs the scan rate derived from the cycling $I-V$ measurements. (c) Galvanostatic charge−discharge curve at a constant current density of 12.5 μA/cm^2. (d) Area-specific capacitance vs current density calculated from charge−discharge curves. (e) Nyquist plot of the AC impedance spectrum of a 2 mm × 2 mm planar capacitor and the fitting curve with a Randles circuit. The AC frequency was varied from 100 kHz to 10 mHz and the amplitude was fixed at 5 mV. The fitted series resistance (R_S) and leaking current resistance (R_L) were 94 Ohm and 7.5 MOhm, respectively, and the capacitance was 1.64×10^{-8} F (i.e., 0.41 μF/cm^2).

dx.doi.org/10.1021/am5006805 | ACS Appl. Mater. Interfaces 2014, 6, 6865−6871

curves are nearly horizontal indicating high Ohmic resistance across the thin Al_2O_3 dielectric film. The small rounded corners, along with the nearly vertical $I-V$ curves at the voltage limits, indicate a low RC time constant and low equivalent series resistance (ESR), which is expected for an electrostatic capacitor.

The area-specific capacitance (C_0) was approximately calculated at each cycling rate using the following equation

$$C_0 = \frac{I_c - I_d}{2Av} \quad (1)$$

where I_c is the charging current and I_d the discharging current at 0 V, v the cycling rate, and A the geometric area of the sandwiched dielectric capacitor. A plot of the area-specific capacitance vs the cycling rate is depicted in Figure 7b. The value is nearly constant for scan rates from 100 V/s to 1000 V/s, indicating the capability of a high power density, which is essential for an electrostatic capacitor.

The area-specific capacitances of the planar capacitors were also determined by galvanostatic charge−discharge cycling at constant current densities. An ideal capacitor shows perfectly symmetric charging and discharging curves with identical time duration. A charge−discharge curve for the annealed planar capacitor at a current density of 12.5 $\mu A/cm^2$ is shown in Figure 7c with duration of ∼9 ms. A small IR drop can be seen at the beginning of each curve due to ESR (<1 kΩ, mostly due to contact resistance) in the circuit.

The area-specific capacitance was further determined by galvanostatic charge−discharge measurements at each current density, J, using the following equation

$$C_0 = \frac{J\Delta t}{\Delta V} \quad (2)$$

where Δt is the charge−discharge time interval and ΔV the voltage window. The slowly decreasing trend of the area-specific capacitance vs current density in Figure 7d is consistent with good dielectric capacitive behaviors revealed by cycling $I-V$ measurements in Figures 7a and 7b.

A Nyquist plot of the annealed planar capacitor and the fitted curve using a Randles circuit are shown in Figure 7e. The frequency of the AC voltage bias was varied from 100 kHz to 10 mHz with a fixed amplitude of 5 mV. The fitted series resistance (R_S, or ESR) and leaking current resistance (R_L) were 94 Ohm and 7.5 MOhm, respectively. An R_L of 7.5 MOhms indicates very high Ohmic resistance across the annealed Al_2O_3 dielectric film. The semicircle symmetry of the spectrum indicates near perfect electrostatic capacitive behavior. The capacitance was calculated to be 1.64×10^{-2} μF, which translates to a specific capacitance of 0.41 $\mu F/cm^2$.

Banerjee et al. reported on a state-of-the-art metal−insulator−metal capacitor using anodic aluminum oxide nanopores coated with a thin layer of TiN (5.5 nm) followed by a thin layer of Al_2O_3 (6.7 nm) and a second layer of TiN (12.6 nm), all via ALD.[7] Two capacitors were constructed at pore depths of 1 μm (A1) and 10 μm (A10) with reported equivalent planar capacitances (EPCs) of 9.9 and 96.0 $\mu F/cm^2$, respectively. The corresponding area-specific capacitances for planar dielectric layers derived from their study are 0.72 and 0.74 $\mu F/cm^2$, respectively. Although the annealed planar capacitor reported here has a lower area-specific capacitance of 0.41 $\mu F/cm^2$, the dielectric constant, k, of the ALD Al_2O_3 layer in this study is actually higher considering the difference in the dielectric thicknesses (20 nm in this work vs 6.7 nm by Banerjee et al.). This work achieved a value of ∼9.3 vs ∼5.5 by Banerjee et al. as calculated from the following equation

$$C_0 = \frac{k\varepsilon_0 A}{d} \quad (3)$$

where ε_0 is the vacuum permittivity and d the thickness of the dielectric layer. Clearly, the quality of Al_2O_3 layer deposited by ALD in this experiment is close to the theoretical value of 9.34 for alumina.[29] In addition, the EPC values reported by Banerjee et al. were obtained using an LCR meter operating at 20 Hz. However, when frequencies of 100 Hz or greater were applied, noticeable dispersion was observed, which greatly decreased the overall capacitance. In this report, the planar capacitor was characterized in great detail using cyclic voltammetry (CV), galvanostatic charge−discharge, and electrical impedance spectroscopy (EIS). CV results (Figure 7a) showed a maximum voltage ramp of 1000 V/s (the high limit of the instrument) in a potential window of 0.2 V in which one full cycle is equivalent to 2500 Hz. For applications that utilize a larger voltage window from −2 to 2 V, it should still have a working frequency of 250 Hz when the same voltage ramp rate is applied. The galvanostatic charge−discharge measurements had a maximum applied current density of 17.5 $\mu A/cm^2$ with a charge−discharge duration of ∼5 ms (or 200 Hz). Neither CV, nor the charge−discharge results in panels b and d in Figure 7, showed any evidence of significant dispersion. The EIS in the full frequency range from 100 kHz to 10 mHz was nicely modeled with the Randles circuit as shown in Figure 7e. Therefore, it is likely that the working frequency could be as high as 100 kHz indicating a large power density. This is the main advantage of a solid-state capacitor over an electrochemical capacitor which is not able to operate at such high working frequencies. The fabrication and characterization of the planar capacitor in this work established a critical step toward our next goal of fabricating a 3D, solid-state VACNF array capacitor. Utilizing the area-specific capacitance from this planar capacitor, and optimizing the growth conditions of the VACNFs and Al_2O_3 dielectric layer, a predicted theoretical capacitance of 83 μF per cm^2 CNFs is possible.

4. CONCLUSIONS

3D VACNF arrays were used as conducting, high-aspect-ratio substrates for ALD coating of AZO/Al_2O_3 double layers. HRTEM imaging revealed that the ALD AZO/Al_2O_3 double layers can form a smooth and conformal shell on VACNF arrays without any prefunctionalization. This uniform growth was achieved along the entire length of the VACNFs from the nickel catalyst tip down to the base. The elemental makeup of the Al_2O_3 core−shell was verified using EDX analysis. HRTEM/SAED images obtained with pre- and postannealed samples revealed that the Al_2O_3 originally grew in an amorphous state on the CNFs and changed to a polycrystalline state after thermal annealing. FESEM images were also obtained in order to show the vertically aligned state of the CNFs uniformity across the substrate. Electrical characterization utilizing planar capacitors confirmed that the Al_2O_3 dielectric deposited by ALD matched the ideal theoretical behavior. This result is important toward the development of high-performance, solid-state capacitors for energy storage.

■ ASSOCIATED CONTENT

Supporting Information

Theoretical capacitance calculation provided for VACNF array capacitor. This material is available free of charge via the Internet at http://pubs.acs.org.

■ AUTHOR INFORMATION

Corresponding Authors

*E-mail: gmalek@ku.edu

*E-mail: jwu@ku.edu

Notes

The authors declare no competing financial interest.

■ ACKNOWLEDGMENTS

The authors acknowledge support in part by NASA Contract NNX13AD42A, ARO Contract W911NF-12-1-0412, and NSF Contracts NSF-DMR-1105986 and NSF-EPSCoR-0903806, and matching support from the State of Kansas through Kansas Technology Enterprise Corporation. We thank Dr. Gaind P. Pandey for his assistance in manuscript preparation.

■ REFERENCES

(1) Jiang, H.; Lee, P. S.; Li, C. Z. 3D Carbon Based Nanostructures for Advanced Supercapacitors. *Energy Environ. Sci.* **2013**, *6* (1), 41−53.

(2) Zhang, L. L.; Zhao, X. S. Carbon-Based Materials as Supercapacitor Electrodes. *Chem. Soc. Rev.* **2009**, *38* (9), 2520−31.

(3) Lytle, J. C.; Wallace, J. M.; Sassin, M. B.; Barrow, A. J.; Long, J. W.; Dysart, J. L.; Renninger, C. H.; Saunders, M. P.; Brandell, N. L.; Rolison, D. R. The Right Kind of Interior for Multifunctional Electrode Architectures: Carbon Nanofoam Papers with Aperiodic Submicrometre Pore Networks Interconnected in 3D. *Energy Environ. Sci.* **2011**, *4* (5), 1913−25.

(4) Liu, J.; Kuo, Y. T.; Klabunde, K. J.; Rochford, C.; Wu, J.; Li, J. Novel Dye-Sensitized Solar Cell Architecture using TiO_2-Coated Vertically Aligned Carbon Nanofiber Arrays. *ACS Appl. Mater. Interfaces* **2009**, *1* (8), 1645−49.

(5) Liu, J. W.; Essner, J.; Li, J. Hybrid Supercapacitor Based on Coaxially Coated Manganese Oxide on Vertically Aligned Carbon Nanofiber Arrays. *Chem. Mater.* **2010**, *22* (17), 5022−5030.

(6) Klankowski, S. A.; Rojeski, R. A.; Cruden, B. A.; Liu, J.; Wu, J.; Li, J. A High-Performance Lithium-Ion Battery Anode Based on the Core−Shell Heterostructure of Silicon-Coated Vertically Aligned Carbon Nanofibers. *J. Mater. Chem. A* **2013**, *1* (4), 1055.

(7) George, S. M. Atomic Layer Deposition: An Overview. *Chem. Rev.* **2010**, *110* (1), 111−31.

(8) Banerjee, P.; Perez, I.; Henn-Lecordier, L.; Lee, S. B.; Rubloff, G. W. Nanotubular Metal-Insulator-Metal Capacitor Arrays for Energy Storage. *Nat. Nanotechnol.* **2009**, *4* (5), 292−6.

(9) Kemell, M.; Ritala, M.; Leskela, M.; Ossei-Wusu, E.; Carstensen, J.; Foll, H. Si/Al_2O_3/ZnO:Al Capacitor Arrays Formed in Electrochemically Etched Porous Si by Atomic Layer Deposition. *Microelectron. Eng.* **2007**, *84* (2), 313−318.

(10) Hirsch, A. Functionalization of Single-Walled Carbon Nanotubes. *Angew. Chem., Int. Ed.* **2002**, *41* (11), 1853−1859.

(11) Banerjee, S.; Hemraj-Benny, T.; Wong, S. S. Covalent Surface Chemistry of Single-Walled Carbon Nanotubes. *Adv. Mater.* **2005**, *17* (1), 17−29.

(12) Farmer, D. B.; Gordon, R. G. Atomic Layer Deposition on Suspended Single-Walled Carbon Nanotubes via Gas-Phase Noncovalent Functionalization. *Nano Lett.* **2006**, *6* (4), 699−703.

(13) Melechko, A. V.; Merkulov, V. I.; McKnight, T. E.; Guillorn, M. A.; Klein, K. L.; Lowndes, D. H.; Simpson, M. L., Vertically Aligned Carbon Nanofibers and Related Structures: Controlled Synthesis and Directed Assembly. *J. Appl. Phys.* **2005**, *97* (4).

(14) Klein, K. L.; Melechko, A. V.; McKnight, T. E.; Retterer, S. T.; Rack, P. D.; Fowlkes, J. D.; Joy, D. C.; Simpson, M. L. Surface Characterization and Functionalization of Carbon Nanofibers. *J. Appl. Phys.* **2008**, *103* (6), 061301.

(15) Lee, J. S.; Min, B.; Cho, K.; Kim, S.; Park, J.; Lee, Y. T.; Kim, N. S.; Lee, M. S.; Park, S. O.; Moon, J. T. Al_2O_3 Nanotubes and Nanorods Fabricated by Coating and Filling of Carbon Nanotubes with Atomic-Layer Deposition. *J. Cryst. Growth* **2003**, *254* (3−4), 443−448.

(16) Herrmann, C. F.; Fabreguette, F. H.; Finch, D. S.; Geiss, R.; George, S. M. Multilayer and Functional Coatings on Carbon Nanotubes using Atomic Layer Deposition. *Appl. Phys. Lett.* **2005**, *87* (12), 123110.

(17) Dhindsa, M. S.; Smith, N. R.; Heikenfeld, J.; Rack, P. D.; Fowlkes, J. D.; Doktycz, M. J.; Melechko, A. V.; Simpson, M. L. Reversible Electrowetting of Vertically Aligned Superhydrophobic Carbon Nanofibers. *Langmuir* **2006**, *22* (21), 9030−4.

(18) Ngo, Q.; Yamada, T.; Suzuki, M.; Ominami, Y.; Cassell, A. M.; Li, J.; Meyyappan, M.; Yang, C. Y. Structural and Electrical Characterization of Carbon Nanofibers for Interconnect via Applications. *IEEE Trans. Nanotechnol.* **2007**, *6* (6), 688−695.

(19) Elam, J. W.; Groner, M. D.; George, S. M. Viscous Flow Reactor with Quartz Crystal Microbalance for Thin Film Growth by Atomic Layer Deposition. *Rev. Sci. Instrum.* **2002**, *73* (8), 2981−2987.

(20) Groner, M. D.; Elam, J. W.; Fabreguette, F. H.; George, S. M. Electrical Characterization of Thin Al_2O_3 Films Grown by Atomic Layer Deposition on Silicon and Various Metal Substrates. *Thin Solid Films* **2002**, *413* (1−2), 186−197.

(21) Elliot, A. J.; Malek, G.; Wille, L.; Mao, B.; Han, S.; Wu, J. Z.; Talvacchio, J.; Lewis, R. M., Probing the Nucleation of Al_2O_3 in Atomic Layer Deposition on Aluminum for Ultrathin Tunneling Barriers in Josephson Junctions. *IEEE Trans. Appl. Supercond.* **2013**, *23* (3).

(22) Lu, R. T.; Elliot, A. J.; Wille, L.; Mao, B.; Han, S. Y.; Wu, J. Z.; Talvacchio, J.; Schulze, H. M.; Lewis, R. M.; Ewing, D. J.; Yu, H. F.; Xue, G. M.; Zhao, S. P., Fabrication of Nb/Al_2O_3/Nb Josephson Junctions using In Situ Magnetron Sputtering and Atomic Layer Deposition. *IEEE Trans. Appl. Supercond.* **2013**, *23* (3).

(23) Miikkulainen, V.; Leskela, M.; Ritala, M.; Puurunen, R. L., Crystallinity of Inorganic Films Grown by Atomic Layer Deposition: Overview and General Trends. *J. Appl. Phys.* **2013**, *113* (2).

(24) Kong, B. H.; Choi, M. K.; Cho, H. K.; Kim, J. H.; Baek, S.; Lee, J. H. Conformal Coating of Conductive ZnO:Al Films as Transparent Electrodes on High Aspect Ratio Si Microrods. *Electrochem. Solid-State Lett.* **2010**, *13* (2), K12−K14.

(25) Elam, J. W.; Routkevitch, D.; George, S. M. Properties of ZnO/Al_2O_3 Alloy Films Grown using Atomic Layer Deposition Techniques. *J. Electrochem. Soc.* **2003**, *150* (6), G339−G347.

(26) Elam, J. W.; George, S. M. Growth of ZnO/Al_2O_3 Alloy Films using Atomic Layer Deposition Techniques. *Chem. Mater.* **2003**, *15* (4), 1020−1028.

(27) Banerjee, P.; Lee, W. J.; Bae, K. R.; Lee, S. B.; Rubloff, G. W., Structural, Electrical, and Optical Properties of Atomic Layer Deposition Al-Doped ZnO Films. *J. Appl. Phys.* **2010**, *108* (4).

(28) Rochford, C.; Li, Z. Z.; Baca, J.; Liu, J. W.; Li, J.; Wu, J., The Effect of Annealing on the Photoconductivity of Carbon Nanofiber/TiO_2 Core-Shell Nanowires for use in Dye-Sensitized Solar Cells. *Appl. Phys. Lett.* **2010**, *97* (4).

(29) Lide, D. R. *CRC Handbook of Chemistry and Physics*, 85th ed.; CRC Press: Boca Raton, FL, 2004.